5. Using AI for tool wear monitoring during interrupted turning of Aluminium

5.1 Introduction

In the previous chapter it was shown how a new method of combining static and dynamic NNs can achieve reliable wear monitoring during hard turning. Although the wear monitoring method is novel, the laboratory setup is similar to other research efforts. The question remains if the method is applicable to industry in terms of its accuracy, reliability and cost-effectiveness. In this chapter, the focus will be on the implementation of the method in industry using cost-effective hardware and appropriate signal processing techniques.

Sick [226] proposed a generic sensor fusion architecture for TCM, consisting of various analogue and digital processing steps. Many research efforts follow more or less this approach, focusing on one, some, or all of the processing levels (described in Chapter 3). However, in recent surveys (see Appendices A and B) of commercial hardware for TCM, it was found that no products are available in the market utilising these techniques. Furthermore, it has been found that not one single commercial TCMS is operational in South Africa. Most manufacturers deem the TCMSs developed up to date too expensive and unreliable. One of the problems identified during the course of this research is the fact that TCM strategies suggested up to date are almost without exception developed and tested on laboratory data. There are two major problems with this approach:

- Laboratory equipment cannot be used on the shop floor (for various reasons).
- The noisy shop floor causes false alarms in a monitoring system developed in a laboratory.

The solution to successful TCM lies in the development of the TCMS with the shop floor conditions in mind. Suggesting a generic structure for the TCMS, and adopting the structure for the specific process, machine, sensors and environmental conditions could achieve this. This chapter describes the experiments and results of an AI monitoring method that was implemented on the shop floor of a piston manufacturer. The method is in principle the same as described in chapter 4, with slight differences in terms of hardware and signal processing. Hence, it will be showed that method described in Chapter 4 under laboratory conditions, can also be applied in industry with slight modifications. The process that is considered here is interrupted turning of an Aluminium alloy during piston manufacture. There are several reasons for this particular choice of operation, the main ones being:

- Industrial need
- It is a turning process with varying depth of cut
- Two different types of cuts are performed, namely facing and boring
- There are similarities between the mechanics of tool wear during interrupted turning and face milling, meaning that the approach could possibly be extended to milling.

5.2 Measurement system

5.2.1 General considerations

Apart from the fact that a TCMS must be designed with the shop floor environment in mind, a further solution to successful TCM lies in *"getting closer to the process"*. The initial selection and placement of sensors is of utmost importance. Tool wear induces very small changes in machining processes. There are also many other obstacles such as diverse failure modes, changing machining parameters and external disturbances that make the task of TCM very difficult.

A sensor that complies with all the TCM sensor requirements (refer to Chapter 3) does not exist. There will always be a trade-off: if the sensor is designed to be as technologically advanced as possible, it will be unaffordable. Manufacturers require a cost-effective solution in order to employ TCM on all their processes. It is universally recognised that force and vibration monitoring can be used for the TCM of turning operations. Often only the static components of the forces are used for TCM. However, using the dynamic components from the force and / or vibration signals can significantly enhance the performance of the TCMS [227]. It has also been shown that some dynamic components are less sensitive to changing machining conditions and external disturbances [6]. Force dynamometers are commonly used in machining experiments (*e.g.* Chapter 4). Although they can measure the static and dynamic forces very accurately, dynamometers are not suitable for the shop floor. Furthermore, their frequency ranges are usually very limited, with a natural frequency f_o (of the piezoelectric parts) at about 3kHz, and a resonant frequency f_r at about 1kHz when clamped. To avoid amplitude distortion, the usable frequency range of a piezoelectric transducer is about $0.6 \times f_o$. For dynamometers commonly used for turning experiments this amounts to about 1.8kHz.

Tramal and Opavsky [228] investigated the dynamics of a conventional force dynamometer for machining operations. It was found that the dynamometer has significant amplitude distortion in the frequency range that is quoted as the operating range by the manufacturer. Unfortunately the authors did not investigate the phase, but it can be assumed that there will be phase distortion as well. The authors suggest that the dynamic characteristics of the dynamometer (while clamped like it would be during measurements) be identified with a modal test and the effect of dynamometer dynamics be compensated for after measurements are made.

Schulz *et al.* [229] recently presented a development of sensor-integrated tool holders. Currently, systems are developed for drilling and milling applications. Forces are measured directly with the mechatronic tool holder with the advantage that the measurement is done close to the cutting edge. The instruments also make use of a flexible telemetric unit for wireless data transfer. Piezoresistive strain gauges are used for estimation of cutting forces. Unfortunately, it is unclear how the system is calibrated and how the clamping and high-speed rotation of the tool holder affects its accuracy. Furthermore, no information about the operational frequency range is given, and it is assumed that the system can only measure static forces. One advantage is an interface of the tool holder directly to the CNC control, which will assist in fast reaction if an undesirable condition is encountered.

It has been found by various authors that the frequencies useful for TCM can be as high as 8kHz, and usually above 1kHz, depending on the experimental setup. A quite simple method to estimate both the static and dynamic components of cutting forces without any distortion is to use resistance strain gauges. Strain gauges comply with most of the requirements for TCM sensors, and can accurately follow the static and dynamic response of a system up to 50kHz. It was therefore decided to develop a sensor-integrated tool holder using strain gauges for this research. Such a system would be cost-effective and could be used on a shop floor. The reader is referred to Appendix C for relevant formation on strain gauges.

5.2.2 Experimental setup

Li and Ulsoy [230] showed how the exact displacement at the tip of a boring bar can determined using strain gauges. Each vibration mode of a beam has its own characteristic gain for converting strain components into displacement, and these are taken into account to determine the beam displacement with submicron precision. The strain gauge measurements can thus be used to determine the exact tool tip displacement during flexible line boring, by using a simulation model.

Santochi *et al.* [103] from the University of Pisa showed how a tool holder could be modified to create a *"sensor-integrated tool"*. Strain gauges were adhered to a standard turning tool holder to estimate cutting forces. The tool holder also contained an amplifying and infrared data transmission unit for wireless data transfer. It was shown that the sensor-integrated tool could be used with relative ease and yields accurate measurements for a range of cutting conditions. A further development of the same tool appeared recently, where radio signals are used instead of infrared, and digital coding of the signal is included [232]. A schematic representation of the sensor-integrated tool developed at the University of Pisa is shown in Figure 5.1.

In this work it was also necessary to develop a similar sensor-integrated tool for use on the shop floor. The main requirements for such a sensor-integrated tool are:

- cost-effective
- robust
- accurate

It will be shown in this chapter that all these requirements were met. Furthermore, in order to obtain a large amount of shop floor data, it was decided to automate the system by making it a data logger that can be controlled and monitored via the Internet. The complete measurement system is schematically depicted in Figure 5.2. The system consists of the following:

- tool holder with strain gauges (3 half-bridges)
- strain gauge amplifiers
- anti-alias filters
- A/D conversion
- computer with data logging software

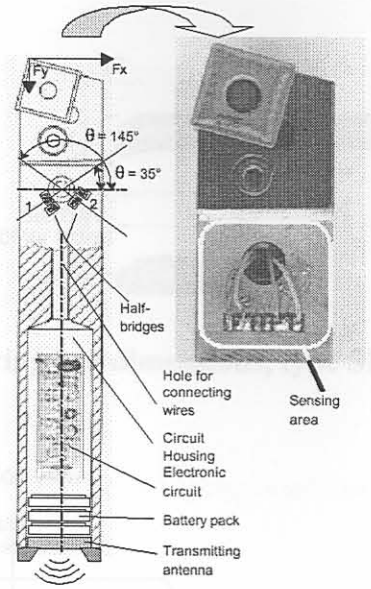

Figure 5.1: Sensor integrated tool [232]

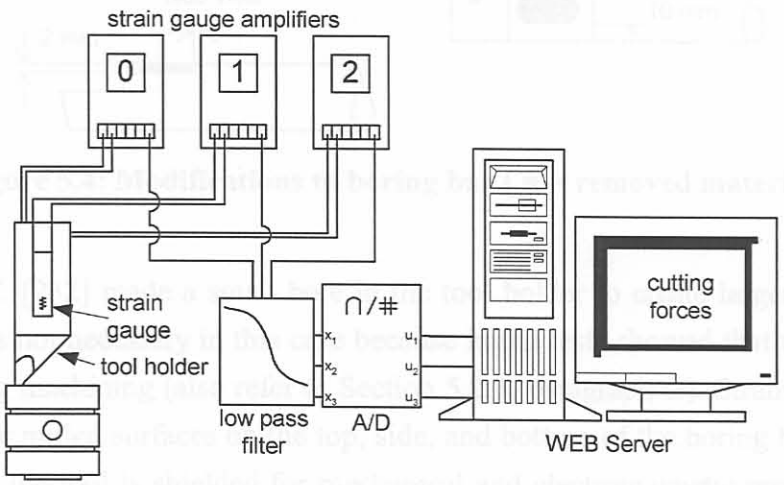

Figure 5.2: Schematic layout of measurement system

The components of the measurement system were either custom designed and built in-house, or were cost-effective commercial products. The complete development of the hardware forms a significant part of the thesis, and more details about the hardware development are given in Appendix E.

5.2.3 Tool holder with strain gauges

Three half-bridges (refer to Appendix C) were constructed on different parts of the tool holder. This creates three measurement channels that can be investigated for sensitivity towards tool wear. Furthermore, channel information should be fused as described in Section 4.6. The tool holder (in this specific case study a boring bar) had to be modified somewhat in order to create flat surfaces for the strain gauges. There was no significant loss of stiffness of the tool due to this modification. The dimensions of the original boring bar are shown in Figure 5.3. An example of the typical modifications is shown schematically in Figure 5.4.

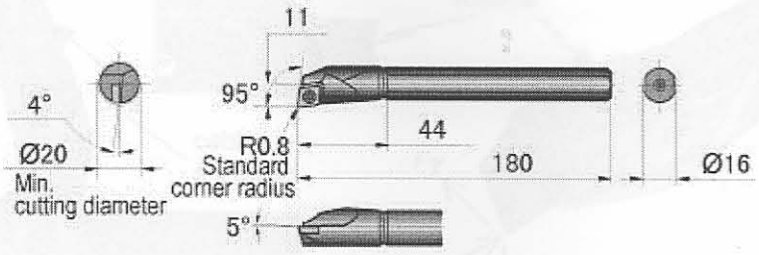

Figure 5.3: Boring bar dimensions, type S16QSCLPR09 [1]

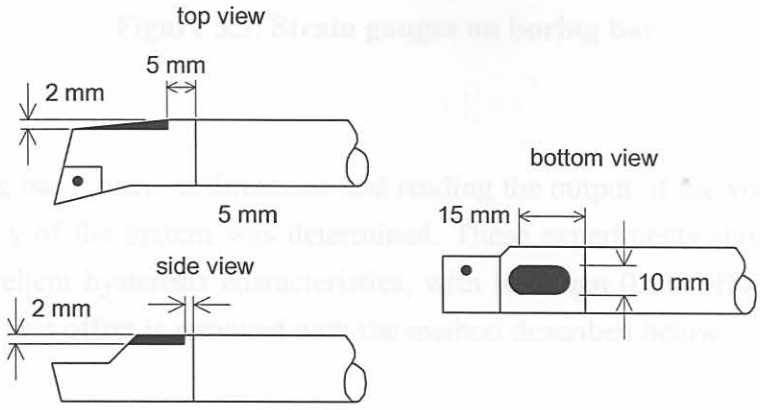

Figure 5.4: Modifications to boring bar (■ = removed material)

Although Failli *et al.* [232] made a small hole in the tool holder to create larger strains (mechanical amplification), it was not necessary in this case because initial tests showed that the strains in the tool are quite large during machining (also refer to Section 5.2.3, paragraph G). Strain gauge rosettes were simply adhered to the milled surfaces on the top, side, and bottom of the boring bar. After application of the strain gauges, the tool is shielded for mechanical and electromagnetic protection. Five sensor-integrated boring bars were manufactured during the course of this work. Pictures of some of the physical layouts of the gauges and shielding material are shown in Figure 5.5. Further information about the strain gauge circuits can be found in Appendices C and E. Some relevant issues with respect to the measurement system are discussed in the following sections.

A. Frequency range of strain gauges

A strain gauge tends to give an integrated average of the strains imposed over its length. The smaller the strain gradient across the element length, the closer the output will be to the true strain. To choose a strain gauge, the desired accuracy of peak strain and frequency extension must be considered. For the tool holder application, 5mm gauges were used, which offer very good accuracy up to 50kHz on steel. A detailed discussion on the electrical resistance strain gauge and how the gauge length should be selected can be found in Appendix C.

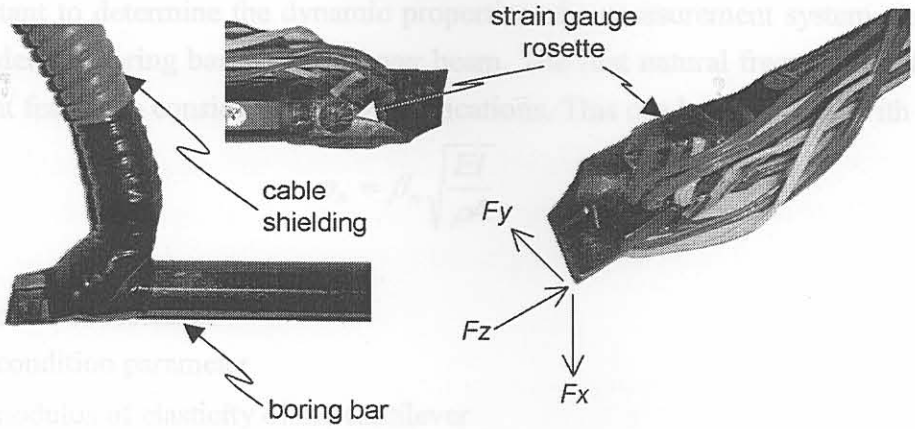

Figure 5.5: Strain gauges on boring bar

B. Hysteresis

By bending the boring bar in various directions and reading the output of the voltages on the channels, the hysteretic accuracy of the system was determined. These experiments showed that the measurement system had excellent hysteresis characteristics, with less than 0.5% offset due to hysteresis effects on all channels. This offset is removed with the method described below.

C. Temperature compensation and drift

Modern-day strain gauges are self-temperature compensated. The strain gauge amplifiers displayed some drift with variations in room temperature. The drift due to temperature effects causes a DC offset in the sensor signals. This offset can be digitally removed from the signal by subtracting the DC values collected when the tool is not engaged in cutting. Care must be taken not to let the system drift into the threshold value for triggering (refer to Section 5.2.7). Experiments were conducted to calculate the drift of the system with variation in room temperature, and the result is shown in Appendix E.

D. Clamping condition

The layout of a typical tool-holder setup is shown in Figure 5.6. The tightening of the clamping screws on the tool holder can cause the holder to bend and cause a DC offset on the measurement channels. The system is zeroed each time when a new tool is clamped, thus removing this effect. The tool holder is in actual fact very seldom removed.

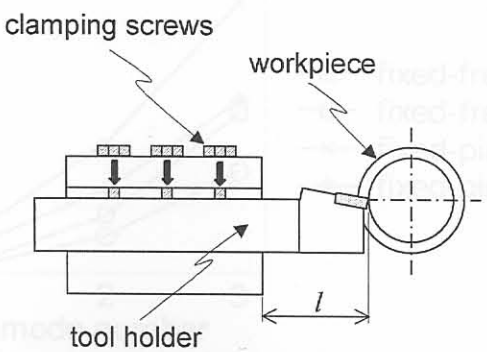

Figure 5.6: Clamping of tool holder

It is very important to determine the dynamic properties of a measurement system. An analytical approach is to model the boring bar as a cantilever beam. The first natural frequency of the cantilever is also an important feature to consider for TCM applications. This can be calculated with [233]:

$$\omega_n = \beta_n \sqrt{\frac{EI}{\rho A}} \tag{5.1}$$

where:

n = the mode of vibration
β_n = end condition parameter
E = the modulus of elasticity of the cantilever
I = the second moment of area
ρ = mass density of tool holder material

β_n is dependant on the length of the overhang of the cantilever (l), and for the first mode in a fixed-free configuration it is given by:

$$\beta_1 = 1.875104 / l \tag{5.2}$$

For a fixed-pinned configuration it is given by:

$$\beta_1 = 3.926602 / l \tag{5.3}$$

The physical difference between the two configurations is diagrammatically depicted in Figure 5.7.

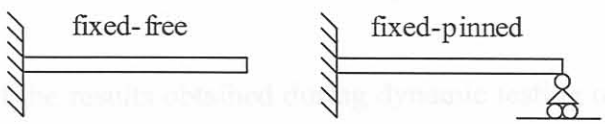

Figure 5.7: Cantilever models

Substituting $\rho = 7850 kg/m^3$, $E = 200 GPa$, $l = 46 mm$, and tool holder radius $r = 16$ mm, the natural frequencies of the cantilever model can be calculated (for the Fx direction) for each new value of l. The result of Equation 5.1 for different values of l and a comparison between a fixed-free and a pinned-free configuration is shown in Figure 5.8. According to this result, the first natural frequency of the boring bar can be expected to be below 10kHz for typical values of l. The higher modes are too high to have any significant influence on the system.

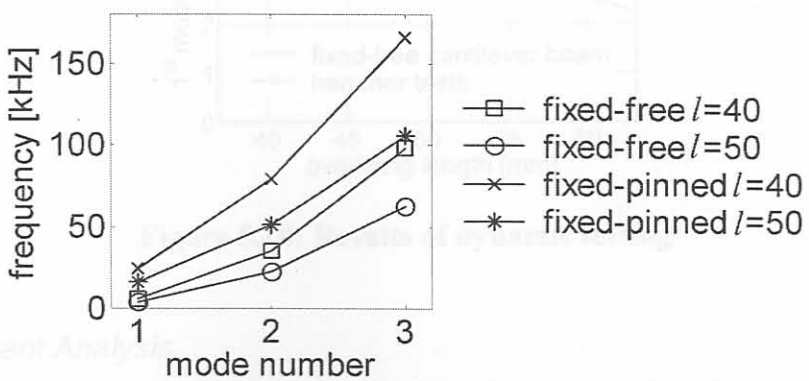

Figure 5.8: Cantilever models natural frequencies

E. Hammer tests

A simple method to experimentally determine the natural frequencies and verify the results described above is to conduct a modal hammer test. When the holder is clamped in position, a modal hammer can be used to dynamically excite the system, and the Frequency Response Functions (FRFs) from the strain gauges can be determined. In this case, the first mode is dominant when excited on the tip of the tool holder with the modal hammer. A picture of the experimental setup for hammer tests is shown in Figure 5.9.

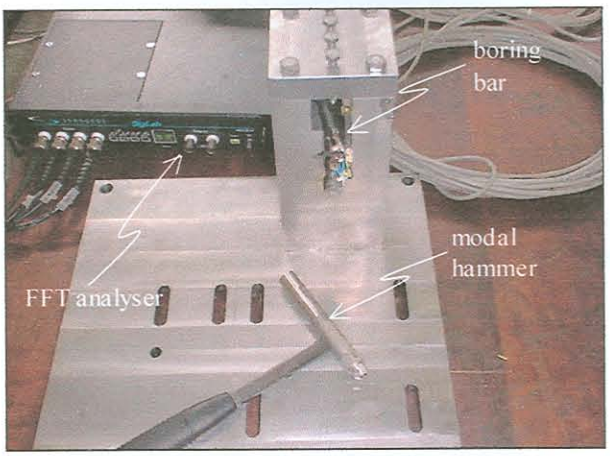

Figure 5.9: Modal hammer experimental setup

Figure 5.10 is a summary of the results obtained during dynamic testing of the sensor-integrated tool. The following conclusions can be made:

- the cantilever model is a rough yet valid estimation method
- the fixed-free cantilever model is the most accurate
- The first natural frequency can be expected to be below 5kHz, probably in the area of 3.5kHz

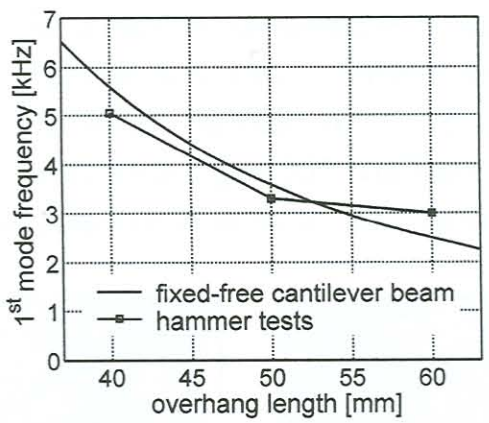

Figure 5.10: Results of dynamic testing

F. Finite Element Analysis

As a further investigation into the dynamic properties of the boring bar, finite element analysis with MSC Nastran was conducted. The automesh function of the software with tetrahedral 10 elements was used. The result of the automesh is shown in Figure 5.11. The aim of the analysis was to:

- verify dynamic tests results
- determine if machining the boring bar has a big influence on the stiffness properties
- determine optimal position to apply strain gauges
- determine the mode shapes

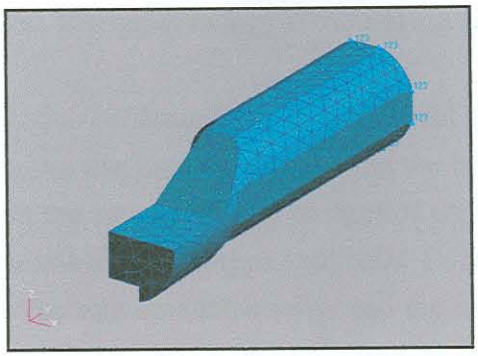

Figure 5.11: Finite element model of boring bar

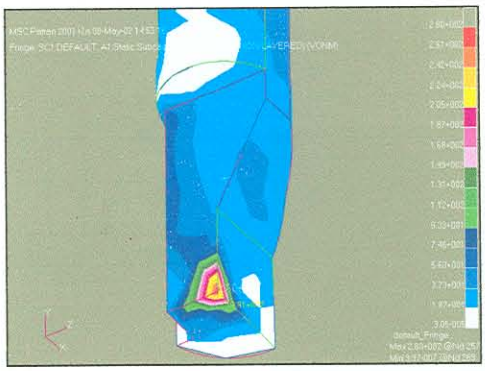

Figure 5.12: Von-Mises stress distribution with load at tool tip

A result of the Von-Mises stress distribution with a typical load on the tool tip is shown in Figure 5.12. Suitable positions for the strain gauges were identified in this way. The stress analysis showed that the machining of flat surfaces had little impact on the properties of the tool holder. Unfortunately, the natural frequencies could not be resolved very well with the model. This can be attributed to the boundary conditions of the clamping which is difficult to model properly. Some of the mode shapes from the finite element analysis are shown in Figure 5.13. The mode shapes also assisted in selection appropriate positions for the strain gauges (refer to Section 4.6.2 on natural frequencies).

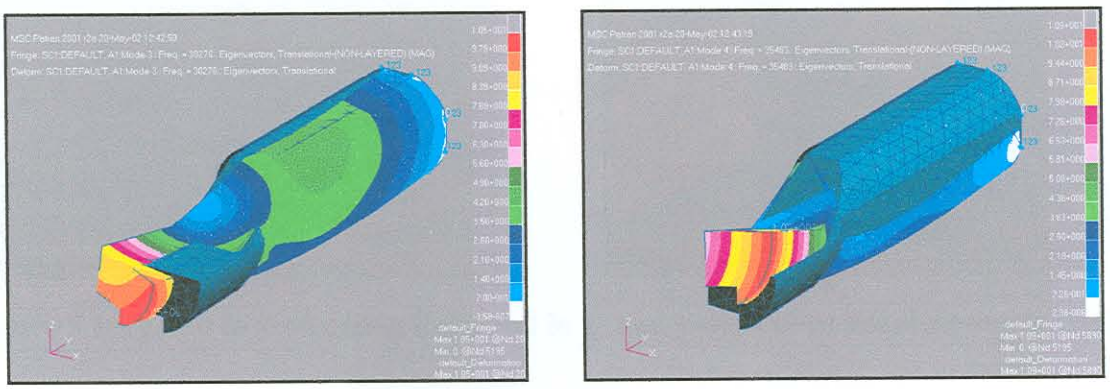

Figure 5.13: Modes three (left) and four (right)

G. Calibration

With the dynamic properties identified, the next step to ensure proper measurements is to perform a static calibration. A matrix of calibration factors for the system can be determined in order to convert voltage into force. Applying known forces to the system and reading the output of the strain gauges will accomplish calibration. In order to calibrate the sensor-integrated tool, a special static calibration test rig was designed and assembled. Design drawings of the test rig are shown in Figure 5.14.

The calibration test rig was designed to calibrate the tool at different overhang lengths. This is possible with an assembly of clamping devices that can also slide along the base plate. By means of a threaded socket on the three mini towers on the rig, forces can be applied on the tool tip in the *Fx*, *Fy* and *Fz* directions. The input forces are measured with Z-type load cells. Consequently, different forces can be applied in the three directions on the tool simultaneously, and the test can be done for any overhang length. The voltage output on the strain gauges is read and these are used to determine a matrix of calibration coefficients. Pictures of typical load cases are shown in Figure 5.15.

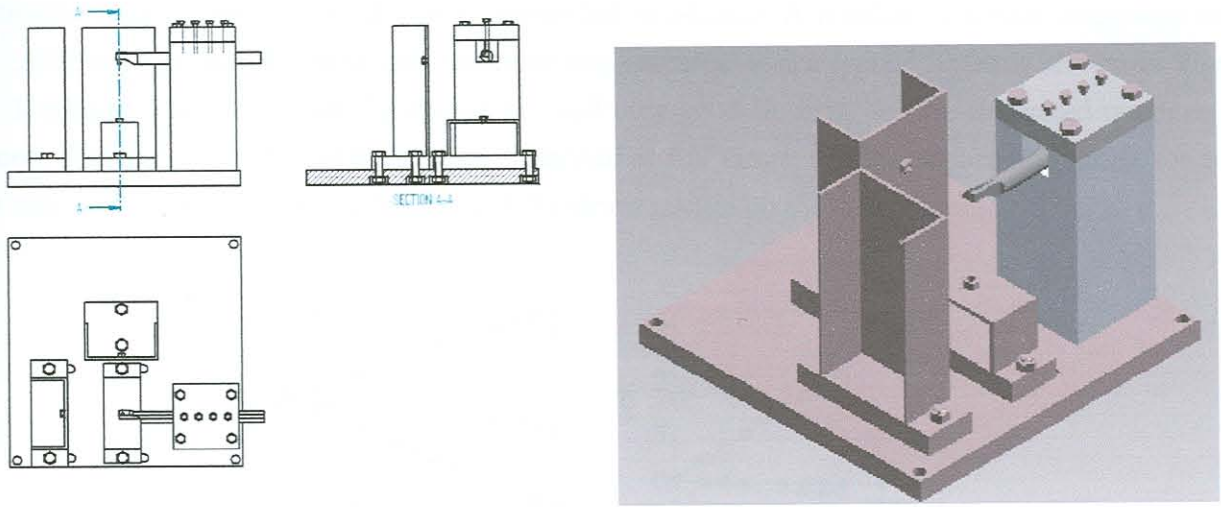

Figure 5.14: Clamped tool on calibration test rig

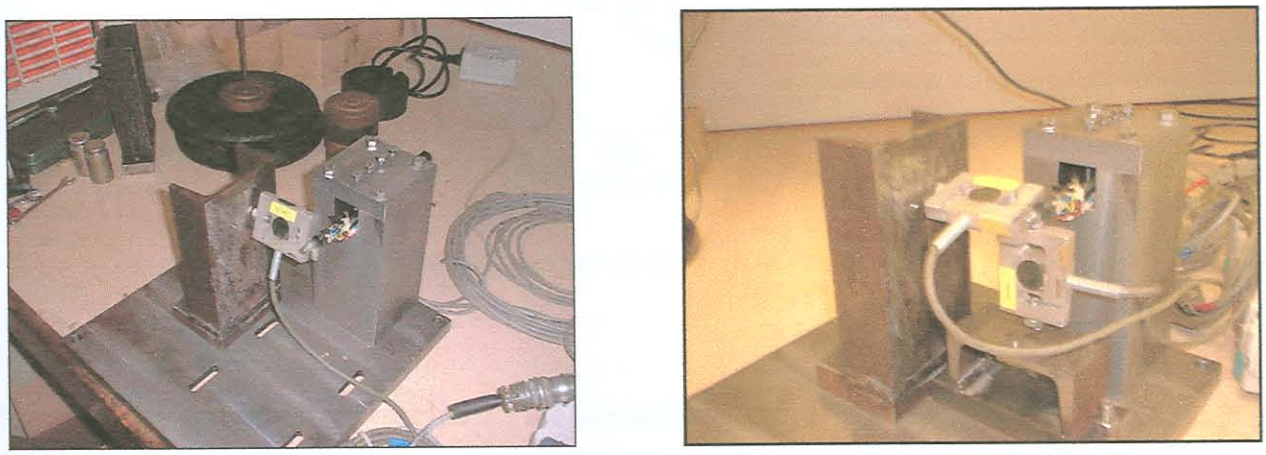

Figure 5.15: Load in y-direction (left) and in x- and y-directions simultaneously (right)

The strain on the tool holder can be related to the force through a linear system written as:

$$\begin{bmatrix} v_1 \\ v_2 \\ v_3 \end{bmatrix} = \mathbf{A} \begin{bmatrix} Fx \\ Fy \\ Fz \end{bmatrix} \quad \text{with } \mathbf{A} = \begin{bmatrix} k_{11} & k_{12} & k_{13} \\ k_{21} & k_{22} & k_{23} \\ k_{31} & k_{32} & k_{33} \end{bmatrix} \tag{5.4}$$

$$\text{or } \boldsymbol{v} = \boldsymbol{Af} \tag{5.5}$$

Matrix coefficients k_{ij} for calibration matrix $\boldsymbol{A}$ can be determined by setting Fx to a known value, and Fy and Fz to zero. For example, setting Fx to 200N:

$$\begin{bmatrix} v_1 \\ v_2 \\ v_3 \end{bmatrix} = \begin{bmatrix} k_{11} & k_{12} & k_{13} \\ k_{21} & k_{22} & k_{23} \\ k_{31} & k_{32} & k_{33} \end{bmatrix} \begin{bmatrix} 200 \\ 0 \\ 0 \end{bmatrix} \text{ yields } \begin{matrix} v_1 = 200k_{11} \\ v_2 = 200k_{21} \\ v_3 = 200k_{31} \end{matrix} \tag{5.6}$$

The measured data can the be calibrated on-line with:

$$\boldsymbol{f} = \boldsymbol{A}^{-1}\,\boldsymbol{v} \tag{5.7}$$

The results of the calibration procedure showed that Fx and Fy could be determined with an accuracy of about 1% for the static calibration range. Fz can be determined with limited accuracy (approximately 15% for static forces) due to the fact that longitudinal stiffness of the tool holder is higher in this direction. The response of Fz is also somewhat non-linear. A number of sensor-integrated tools were calibrated and tested during the course of this research, and a typical result is shown in Figure 5.16. The calibration of Fx and Fy always showed very good linearity for the calibrated range on all channels. The sensor-integrated tools were calibrated at full range, and the calibration matrix for each too is unique due to the shape and location of the strain gauges on the tool holder.

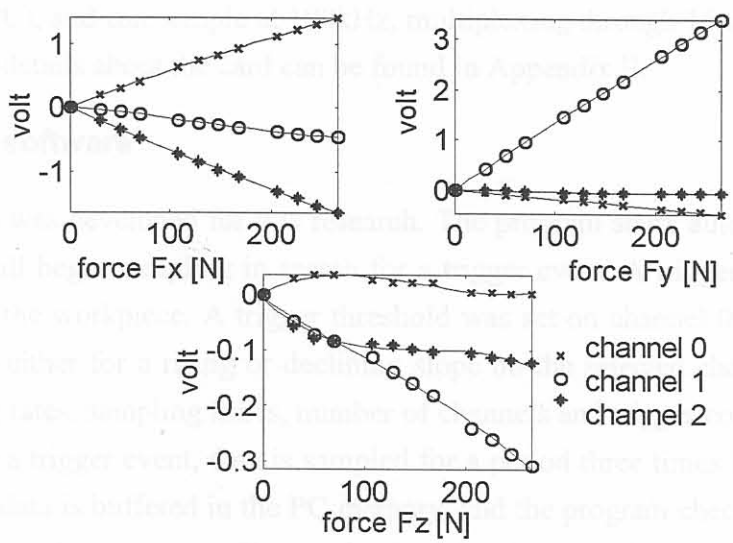

Figure 5.16: Calibration result for one of the developed tools

5.2.4 Strain gauge amplifiers

The purpose of the amplifiers is to excite the Wheatstone bridge used for strain gauge measurements. The amplifiers provide the voltage over the full-bridges and also have a zero-pod and a digital read-out unit. One consideration when choosing a strain gauge amplifier is the frequency range of the amplifier. The usable range of the amplifiers used for this application is DC – 6kHz. More information can be found in Appendix E.

5.2.5 Anti-alias filters

A very important consideration when sampling dynamic signals is the phenomenon of aliasing. Aliasing can only be prevented by:

- Using a sampling rate (F_s) of at least twice the bandwidth (BW) of interest.
- Using an analogue anti-alias filter with corner frequency at BW.

Versatile analogue filters are available commercially, though at a very high price. Furthermore, commercial filters are usually designed for laboratory work and it cannot be afforded to leave them permanently on the shop floor. Therefore it was decided to build an anti-alias filter in-house, with the help of the *Filterlab Low-pass* software from Microchip [234]. More details on the filter development are available in Appendix E.

Three identical channels were built to pass DC - 4000Hz, with the -3dB point at approximately 4350Hz. A sampling frequency of 20kHz is suggested when using the filter to prevent aliasing in the DC – 4kHz band. However, the filter has significant phase distortion on analogue signals. This characteristic can be rectified digitally by creating an identification model of the filter. An Autoregressive (AR) time series model was made from identification data of the filter. This model is then saved and all measured data are then reversed through the model to compensate for the phase distortion.

5.2.6 A/D conversion

A/D conversion was done with a 12-bit card from Eagle Technologies (PC-30). The card slots into a Personal Computer (PC), and can sample at 100kHz, multiplexing through 16 single-ended or 8 differential channels. More details about the card can be found in Appendix E.

5.2.7 Data logging software

Special C++ software was developed for this research. The program starts automatically when the PC is powered on, and will begin sampling in search for a trigger event. A trigger event will occur when the tool engages into the workpiece. A trigger threshold was set on channel 0 at +0.05V. The trigger can be selected to be either for a rising or declining slope on the selected channel. The user can initially set the sampling rates, sampling times, number of channels and trigger conditions on a web page. During the search for a trigger event, data is sampled for a period three times longer than the selected sampling length. The data is buffered in the PC memory, and the program checks it for a trigger event. If a trigger event occurs, the program will save the data for the user-selected period. The program can also be instructed to save only every 10^{th}, 20^{th} or N^{th} trigger event, as not to save the data for every workpiece. Each file is saved with a time stamp. As a last step, after a number of data files were collected, they are stored in a compressed format to save disk space. The compressed files are then available for download through the Internet. The program settings can also be changed remotely via the Internet. On the shop floor, a person is responsible for logging tool changes and safekeeping the tools for later investigation under a microscope. For some tool inserts regular wear measurements were made. Each machined part is also automatically logged and time stamped on the shop floor and can thus be correlated with the recorded data. A flow diagram of the program is shown in Figure 5.17. The

complete system was installed in a steel enclosure, shown standing on the shop floor in Figure 5.18. A screen capture of the web page where the program setting are submitted in shown in Figure 5.19, and a screen capture of the logger in operation is shown in Figure 5.20.

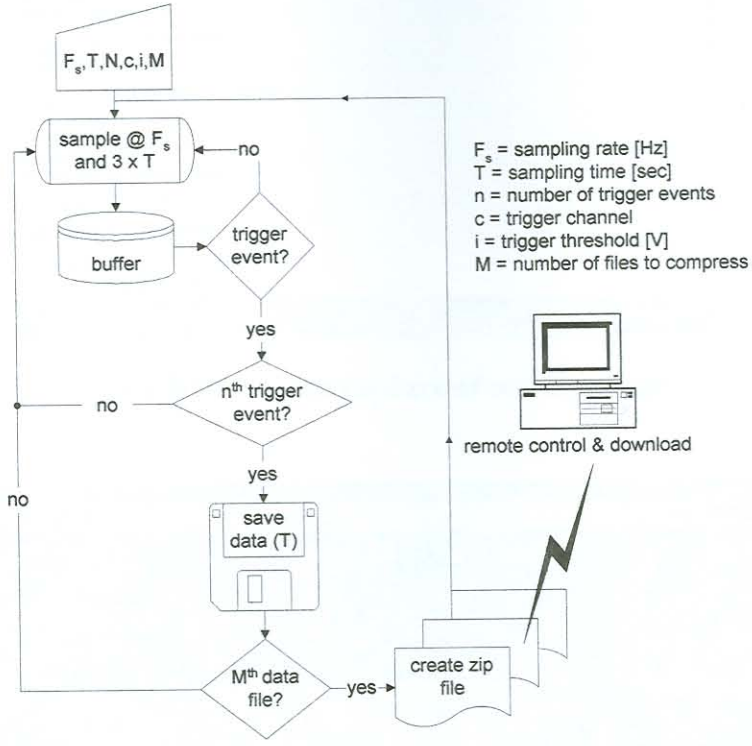

Figure 5.17: Flow diagram of data logging program

Figure 5.18: Steel enclosure for monitoring electronics

5.3 Cost breakdown

Cost-effectiveness was a very important consideration for the development, due to the various reasons stated in earlier chapters. The approximate cost of the individual components are summarised in Table 5.1. The total cost (hardware and software) of the system amounts to about €1000. This is significantly lower than any commercial measurement system available today.

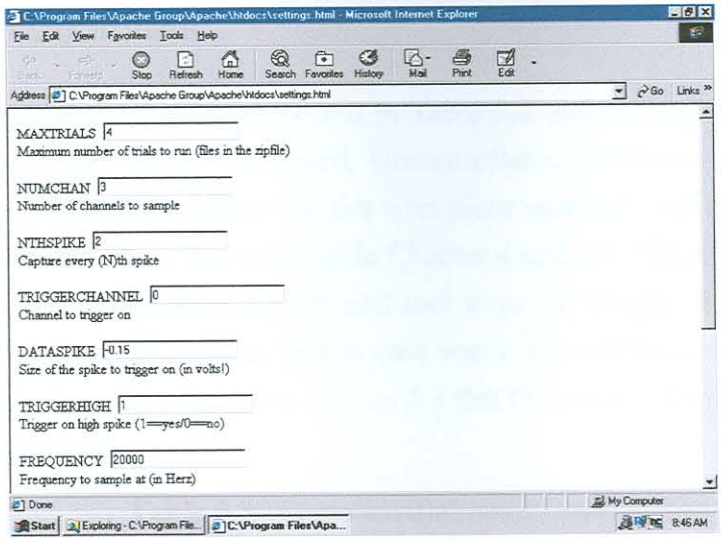

Figure 5.19: Screen capture of settings page

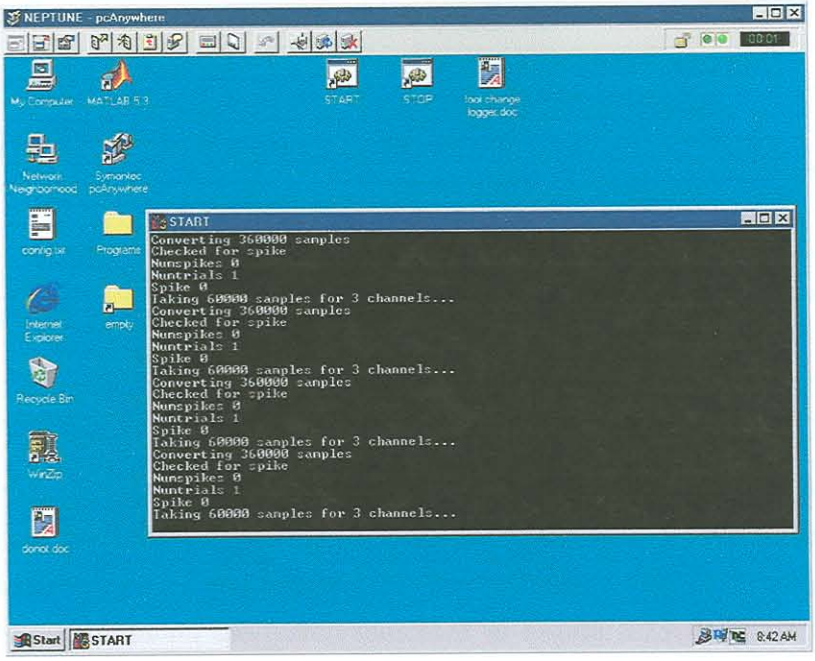

Figure 5.20: Logger in operation

Table 5.1: Cost breakdown of measurement system

boring bar	€ 80
strain gauges	€ 70
shielding material	€ 80
strain gauge amplifiers	€ 150
anti-alias filter	€ 20
A/D card	€ 100
computer (Pentium @ 200MHz)	€ 250
software	€ 100
miscellaneous costs	€ 150
Total	**€1000**

5.4 Experimental conditions

The basic experimental conditions are summarised in Table 5.2. All controllable conditions remained the same except the feed rate, which was varied. Uncontrollable conditions refer to external disturbances such as shop floor vibrations, softer / harder workpiece material, tool quality *etc*. These disturbances were more chaotic than those encountered in Chapter 4 and it is virtually impossible to investigate their individual effects on the force signals and tool wear. In Chapter 4 the effects of identified disturbances were filtered from the signals. In this case was not possible. However, despite the noisy nature of the environment, it will be shown in Section 5.7 that the proposed wear monitoring method is robust towards these conditions.

Table 5.2: Experimental conditions

machine	feed rate	0.3 mm/rev and 0.2 mm/rev
	cutting speed	390 m/min
	depth of cut	variable 1.7 mm max
	tool holder	S16 QSCLPR 09
	insert type	CCGT 09T304 FN-ALU (carbide)
	workpiece	Aluminium alloy (confidential)
strain gauges	3 half-bridge configurations	
	type	KYOWA KFG-1-120-D17-11
	amplifier	HBM clip® System
filter	custom made cut-off at 4 kHz	
A/D card	Eagle Technologies PC-30	
	sampling rate	20 kHz per channel
	sampling time	3 seconds per channel

The machine on which experiments were conducted is depicted in Figure 5.21, with a picture of the sensor cable exit from the machine in Figure 5.22. Some pictures of the sensor-integrated tool in operation are shown in Figure 5.23 and Figure 5.24. The operations that were considered consisted of a facing and boring on the areas on the piston indicated in Figure 5.25. It is a crucial section on the workpiece with respect to geometric accuracy and hence monitoring of the tool wear is essential. Due to the interrupted character of the cut, the tools also tend to wear fast. More details on the tool wear will follow in Section 5.5.

Figure 5.21: Turning machine

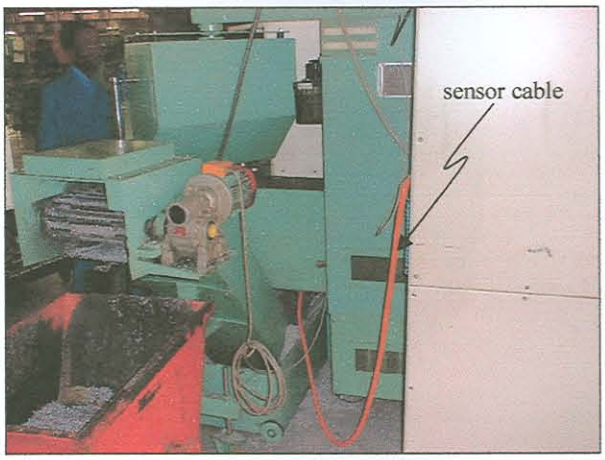

Figure 5.22: Cable exit

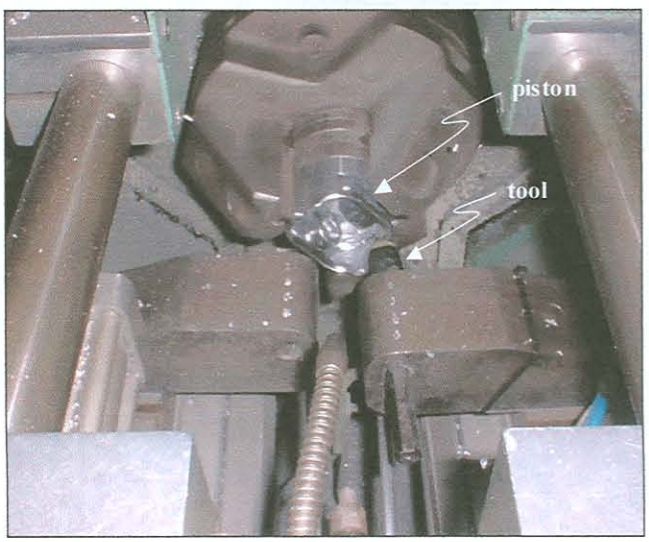

Figure 5.23: Sensor-integrated tool in operation (1)

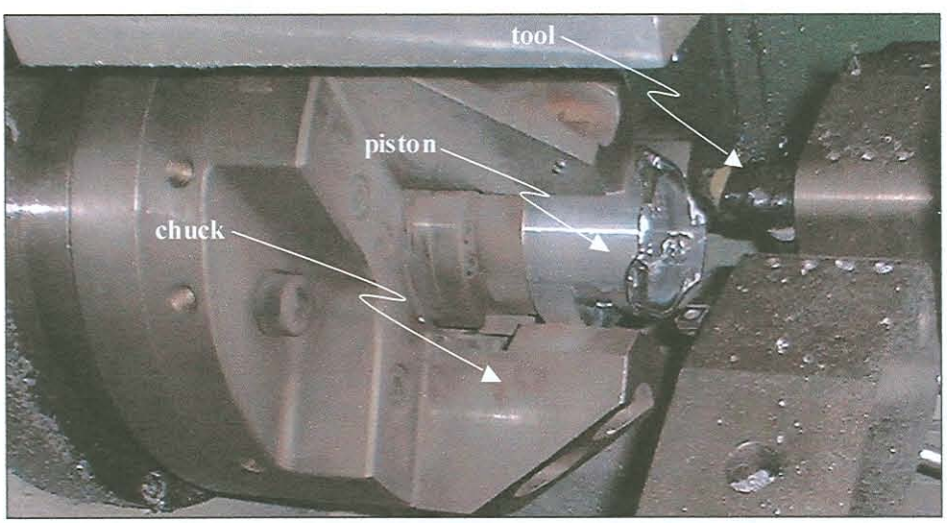

Figure 5.24: Sensor-integrated tool in operation (2)

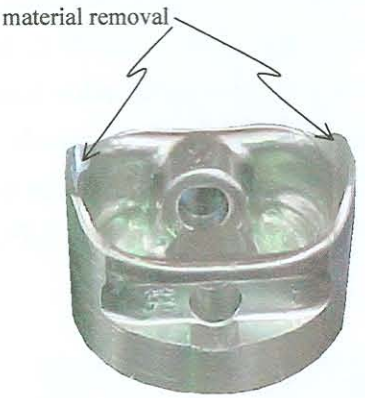

Figure 5.25: Workpiece

5.5 Tool wear

Before further analysis of the signals can be discussed, some remarks about the tool wear must be made. During the course of the research, data from almost 100 tool inserts were collected. This implies that force signals from the process were collected continuously from a new to a worn tool insert for many tools. The experience from the operators on the shop floor is that the tool wear is unpredictable. Sometimes a tool will last for thousands of components, and sometimes it will wear out after a few hundred. A conservative approach is used to eliminate the possibility of scrapping a part and tools are often replaced long before they have to be. The unpredictability of the tool wear was confirmed with wear measurements on the shop floor. A comparison of the flank wear of several tools with respect to the number of components that were machined with them is shown in Figure 5.26. It can be seen that the rate of tool wear is slightly different for every case, despite the fact that controllable conditions were kept constant.

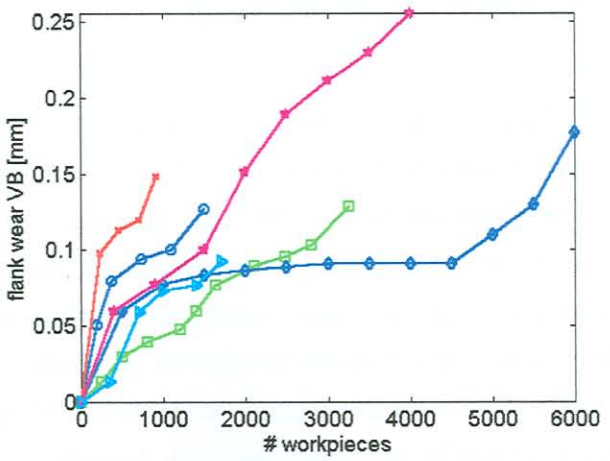

Figure 5.26: Tool wear with respect to number of machined workpieces

Reasons for this fluctuation in tool life can be attributed to conditions on the shop floor. More specifically, the rate at which components are manufactured plays a significant role. If the time allowed for the tool to cool down between runs is not kept constant, large variations in tool life can be expected. Fluctuations in the workpiece composition can also play a large role but is extremely difficult to quan-

tify these effects. A very significant conclusion from this is that tool life equations (*e.g.* modified Taylor equations [42]) cannot solve the problem in this case, hence justifying the need for an on-line TCMS. For all wear measurements and subsequent wear estimation, the average flank wear over a selected area of the cutting insert was chosen as a representative value of the tool condition. In order to obtain a closer understanding of the tool wear, Scanning Electron Microscope (SEM) pictures were taken of several used inserts. An SEM photo of a new insert is shown in Figure 5.27, compared to worn inserts in Figure 5.28.

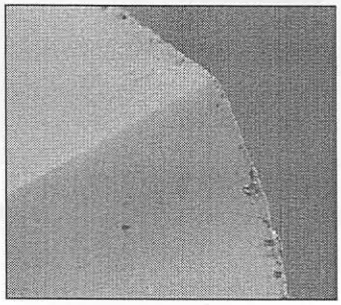

Figure 5.27: New insert

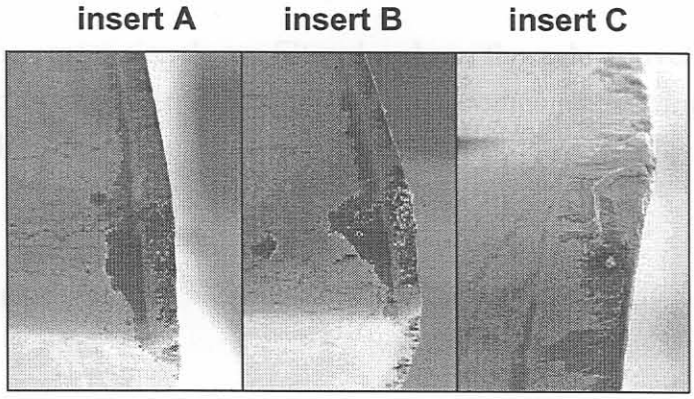

Figure 5.28: Worn inserts

Though the basic wear modes on the tools are similar, the geometry or shape of the wear land is different for each case. Similar observations were made with other worn tools under the SEM. From the SEM investigations it was concluded that the wear on the tools generally consisted of a plastic flow and an elastic contact region. There are also signs of micro-chipping and cracking at the edge, especially with severely worn tools. It was furthermore concluded that the chosen wear parameter of flank wear is adequate for describing the severity of wear on tool, because it has the most significant effect on the workpiece quality. Micro-chipping occurs at a late stage of the tool life, and it is virtually impossible to determine the effect of different severities of micro-chipping on part quality due to the large degree of flank wear also present. An example of the different wear modes on the tool is shown in Figure 5.29. The plastic flow and elastic contact zones form the total flank wear.

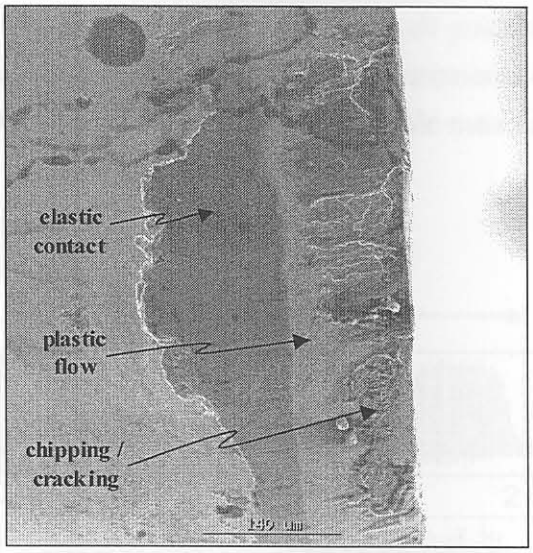

Figure 5.29: Different wear regions

5.6 Signal processing

5.6.1 Pre-processing

In the analogue form, the sensor signals are filtered and run through an overload protection unit. The aim of the digital pre-processing is to obtain reliable three-component cutting forces from the voltage values measured by the hardware. The following steps are taken:

- phase correction
- resampling
- DC offset compensation
- calibration

The phase correction is necessary due to the phase distortion caused by the analogue filter. Phase correction is done through an appropriate identification model of the filter, as discussed in Section 5.2.5. A high sampling rate must initially be used to prevent aliasing in the analogue format, but resampling makes the signals easier to process in digital format because of the lower file size. The process of resampling also involves digital low-pass filtering at half the new sampling rate. The signals were resampled to an effective sampling rate of 8kHz. The DC offset is removed with a reference signal collected when the tool is not engaged into the workpiece. A typical force measurement after the preprocessing step is shown in Figure 5.30. The cut essentially consists of two parts corresponding to a facing (A in the figure) and boring process (B in the figure). The feed direction is thus in the y-direction for A and in the z-direction for B. Due to the nature of the process, only section B of the signal contained information on the flank wear. The shape of the signals are due to the process, which is an interrupted cut with varying depth of cut and effective angles (resulting from the workpiece geometry).

The frequency of interruption is exactly 50Hz. It can be seen that this particular section actually creates positive and negative forces in the *Fy* direction, which is once again caused by convex shapes on the workpiece during the boring process. The cutting forces can now be analysed digitally to assist in the

design of a strategy to accurately monitor the process, with all possible internal and external disturbances. The system was set to store approximately 100 measurements during the life of a single tool. This would represent about 10% of the total number of possible measurements, but is still a sufficient amount of data.

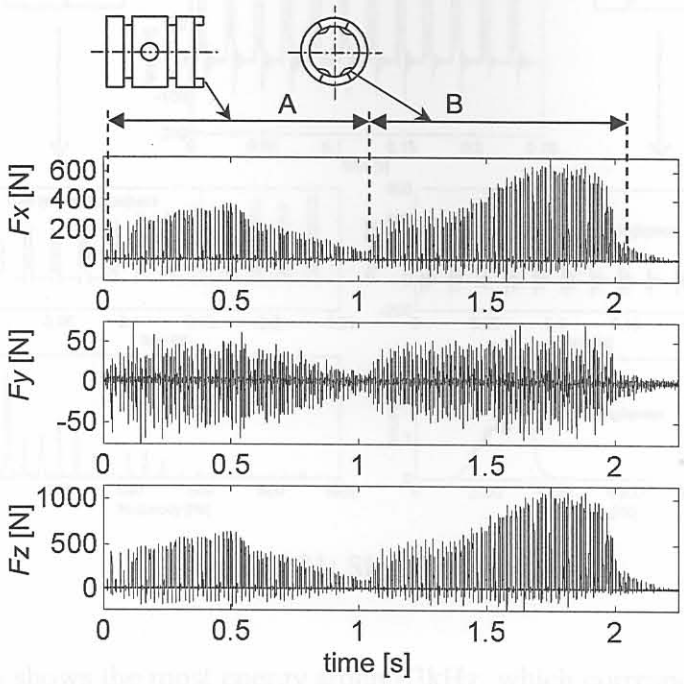

Figure 5.30: Typical cutting forces

5.6.2 Signal investigation

In order to identify possible signal features that might correlate with tool wear, several investigations were conducted. The signal basically consists of a low frequency region that is an indication of the static cutting forces. In the higher frequency range, the tool holder natural frequencies are observed because the cutting process excites them. Such a distinction of the two frequency ranges is shown in Figure 5.31. The spectrum in the lower range reveals many harmonics of the fundamental frequency of interruption, which is expected due to the square shape of the signal caused by the interrupted cut. Both these frequency ranges could contain information on the tool wear, but the type of analysis to be performed would differ for each range. Other initial signal investigation included time-frequency analysis to determine if there are certain frequencies increasing in amplitude with time. It is obvious that this will be the case due to the increasing and decreasing depth of cut. Hence, a particular section of the signal was selected for all subsequent analyses.

5.6.3 Feature extraction

The next step is to identify and extract features from the signals that are sensitive to tool wear. The static component of the force signal is represented in the 50Hz (and harmonics) component of the FFT. Thus, features representing the energy of the 50Hz component and its harmonics were generated as possible features. From initial investigations, it seemed that especially the 100Hz and 150Hz regions could be reliable features for TCM. A Cepstrum analysis was also carried out to see if the harmonics of 50Hz can be represented in a single parameter, but this did not yield a significant improvement.

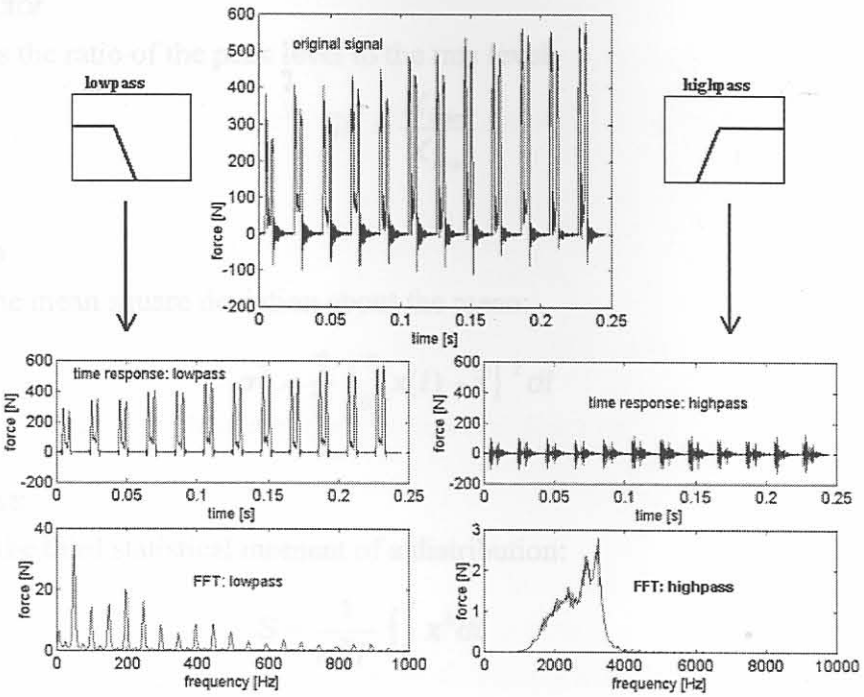

Figure 5.31: Signal character

The high-pass filtering shows the most energy around 3kHz, which corresponds to the tool holder cantilever natural frequency in the direction of *Fx*. These frequencies are often useful for TCM. The frequency spectrum was investigated in detail for frequency bands sensitive towards tool wear. This can be done by selecting certain frequency bands and calculating the energy contained within it. The energy in a frequency band can be expressed as:

$$\psi^2 = \int_{fl}^{fh} S_y df \tag{5.8}$$

with S_y the one-sided PSD function of the force signal and *fl* and *fh* chosen to reflect the energy in the regions of interest. Some simple time domain parameters were calculated as possible features, such as maximum and minimum values, peak-to-peak values, zero crossings and others. More common features often used for TCM applications in the literature were also calculated, which include:

A. Mean

The mean value of a function *x(t)* over an interval T is:

$$\bar{x} = \frac{\int_0^T x(t)dt}{T} \tag{5.9}$$

B. Root mean square (rms)

The rms value of a function *x(t)* over an interval of T is:

$$X_{rms} = \sqrt{\frac{\int_0^T x(t)^2 dt}{T}} \tag{5.10}$$

C. Crest factor

The crest factor is the ratio of the peak level to the rms level:

$$CF = \frac{X_{max}}{X_{rms}} \tag{5.11}$$

D. Variance

The variance is the mean square deviation about the mean:

$$\sigma^2 = \frac{1}{T}\int_0^T [x(t) - \bar{x}]^2 dt \tag{5.12}$$

E. Skewness

The skewness is the third statistical moment of a distribution:

$$S = \frac{1}{\sigma^3 T}\int_0^T x^3 dt \tag{5.13}$$

F. Kurtosis

The kurtosis is the fourth statistical moment of a distribution:

$$K = \frac{1}{\sigma^4 T}\int_0^T x^4 dt \tag{5.14}$$

G. Time series model features

Time series models can also be used to monitor a process, where the model coefficients are used as features. The model coefficients represent the characteristic behaviour of the signal. Depending on the order of the model, a number of model coefficients can be chosen. Normally only the first model coefficient, or sometimes the first three to four model coefficients are chosen because they are most descriptive of the signal [53,121,207]. Higher coefficients can actually become descriptive of noise within the signal, and therefore they are not preferred as wear monitoring features.

For the purpose of this research, the first coefficients from the Auto Regressive (AR) model, Moving Average (MA) model, and the Auto Regressive Moving Average (ARMA) model, were used as features for tool wear estimation. The models are calculated directly from the calibrated force signals. A brief discussion of each of the models follows [235-237]:

AR model

In a p-th order AR model for a time series $x(n)$, where n is the discrete time index, the current value of the measurement is expressed as a linear combination of p previous values:

$$x(n) = a_1 x(n-1) + a_2 x(n-2) + \ldots + a_p x(n-p) \tag{5.15}$$

where $a_1, a_2 \ldots a_p$ are the AR coefficients. The first AR coefficient was chosen as a feature.

MA model

In a q-th order MA model, the current measurement is expressed as a linear combination of q previous values from a sequence of Independent Identically Distributed (IID) random variables with a certain

probability density function.

$$x(n) = b_1 u(n-1) + b_2 u(n-2) + \ldots + b_q u(n-q) \tag{5.16}$$

where $b_1, b_2 \ldots b_q$ are the MA coefficients and $u(n)$ is assumed to be an IDD sequence. The first MA coefficient was chosen as a feature.

ARMA model

The ARMA model is a combination of the above two models:

$$x(n) = -\sum_{k=1}^{p} a_k (x(n-k)) + \sum_{k=1}^{q} b_k (u(n-k)) \tag{5.17}$$

The first two coefficients from this model were chosen as features.

5.6.4 Feature selection

A. Methods

With a list of possible features for TCM generated, a selection of the most reliable features must be made. This is one of the most important steps in designing a TCMS. There are various methods for feature selection and feature space reduction. In the case of feature space reduction, a method is applied that will reduce the dimensionality of the feature space. A popular way to achieve this is by means of Principal Component Analysis (PCA) [6]. The method of PCA calculates the eigenvectors of the feature matrix and re-aligns the feature matrix into its orthogonal dimensions. However, in the case of TCM, the input space (or the original feature matrix) is often one-dimensional because the best features tend to increase monotonically with tool wear. The PCA method was subject to further investigation and is discussed in Chapter 6.

Another method is to reduce the number of features by selecting the features that correlate the best with the objective (tool wear). There are a number of methods to achieve this. A very simple method is the use of the correlation function between the feature and the objective. If a particular feature displays a repeatable tendency towards high correlation with tool wear it can be selected as a feature for TCM. The correlation coefficient (expressed as a percentage) between the selected feature q and tool wear V can be calculated as follows:

$$\rho = \left| \frac{\sum_i (q_i - \bar{q})(V_i - \bar{V})}{\sum_i (q_i - \bar{q})^2 \sum_i (V_i - \bar{V})^2} \right| \times 100 \tag{5.18}$$

where $\bar{q}$ and $\bar{V}$ are the means of q and V, respectively; ρ is the correlation coefficient of which the value indicates linearity between q and V. When ρ is approaching 100%, there exist a relationship between q and V. The lower the value of ρ, the lesser the chance for the selected feature to show any trend towards tool wear.

Another method that was investigated as a possible method for feature selection is by means of a Genetic Algorithm (GA). The GA is an algorithm often used for discrete optimisation problems. Its formulation is based on the principles of natural selection. A detailed discussion of GAs is beyond the scope of this text, but more information can be found in [238]. For the purpose of feature selection, an optimisation problem can be formulated with the objective to select the optimal population of features

to estimate tool wear. Furthermore, the features can be automatically ordered from the best to the worst choice.

Both methods for feature selection were used during the course of this research. The methods always yielded similar results, but the GA is computationally much slower than the simple correlation coefficient approach. If feature selection must be done on-line, the GA approach is probably not the best choice. Furthermore, a GA must always be run more than once. In fact, it must be run at least three times to verify the result. The simple correlation coefficient approach is a simple alternative that is also feasible for on-line implementation (refer to Chapter 6).

As a last step of feature selection, some engineering judgement is required. The reason for this is that the automatic methods will often select features that are too similar or dependant on one another, and thus not achieving the goal of proper sensor fusion. In this case, the rules for selecting features based on engineering judgement can be stated as:

- Select features from the static and dynamic parts of the signal
- Select features from the different force directions
- Use time and frequency domain features
- Features based on simple signal processing methods are preferred
- There should be a reasonable physical explanation for the behaviour of a feature with respect to tool wear

It should be mentioned here that features were not investigated for insensitivity towards changing machining parameters. It has been shown that machining parameters can be included in the method and hence the behaviour of a feature with respect to machining parameters is irrelevant, the only requirement being that the feature remains sensitive towards tool wear when a machining parameter varies. The chosen features remained sensitive towards tool wear irrespective of machining parameters.

B. Selected features

It was found that the data from the shop floor is extremely noisy and that most features do not display any correlation with tool wear. However, a list of possible features was identified using the methods described above. As a last step engineering judgement was applied in selecting the following features:

Table 5.3: Description of features

feature	*description*
Fxs	standard deviation of *Fx*
Fxd	spectral energy of *Fx* at mode one (approx 2kHz)
Fym	mean of *Fy*
Fy50	energy around 50Hz for *Fy*

A plot of the chosen features with respect to tool wear (interpolated) is shown in Figure 5.32. Note that the features are always normalised for modelling purposes. It is clear from the figure that although the features tend to increase with increasing tool wear, the trend is far from consistent. There is a large degree of variance in the feature trend and the correlation with the true tool wear is rather poor.

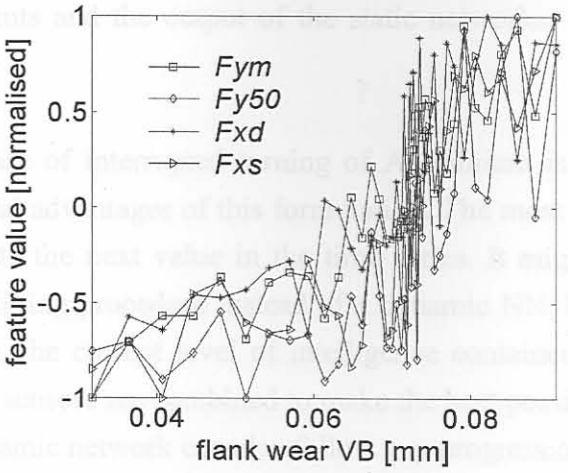

Figure 5.32: Normalised features

Some physical explanations for the increasing trend in the features are necessary. The standard deviation of *Fx* represents the vibration energy contained within the signal. In this case, the static cutting force will dominate this value, and one can conclude that the standard deviation increases due to an increase of the static force and to a lesser extent an increase in higher frequency vibration. The forces increase due to an increase of friction between the tool tip and workpiece when the tool flank is worn. The dynamic parameters in this case are governed by the harmonics of the interruption frequency and also by the dynamic behaviour of the tool holder in the *Fx* direction. The excitation from the cutting process causes the holder to vibrate freely at its natural frequency, and the vibration amplitudes in this range normally increase with increasing tool wear. The increase is once more caused by the larger impacts on the tool tip due an increase of friction between the tool and the workpiece. The parameters generated from the *Fy* force are both more representative of the static cutting forces, and the same arguments apply. Some information about the vibration energy in the *Fy* direction is contained in the *Fym* feature.

Due to the high degree of variance in the increasing trends of the features, a monitoring strategy based on any one of the features alone will never yield an accurate estimation of the tool wear. For this reason, an AI approach is used to estimate these values. The approach is exactly the same as that applied to hard turning in Chapter 4. The selected four parameters are sufficient to monitor tool wear because there are no other changes to the process, *e.g.* workpiece or tool type. If such disturbances were present, it would in all probability be necessary to include other features as well. During the experiments, two different feed rates were used, but the selected features applied for both feed rates.

5.7 AI method for TCM

The tool wear can be classified by using the selected features as inputs to an AI model. The principle of the AI approach proposed in this work relies on the use of a series of NNs, one of which is trained on-line and others that are trained off-line. The off-line networks are static networks that are trained to model the feature values for known values of tool wear and cutting conditions. The on-line network is a dynamic network that attempts to estimate the current wear on the cutting edge by using the previous estimations of tool wear as inputs. The training goal for the dynamic network is to minimize the error

between on-line measurements and the output of the static networks. This is the same method presented in Section 4.6.3.

The AI approach for the case of interrupted turning of Aluminium is diagrammatically depicted in Figure 5.33. There are several advantages of this formulation. The most important is in the use of temporal information to estimate the next value in the time series. It might seem possible to achieve a similar result with a curve fitting procedure instead of a dynamic NN, but the problem is much more complex. With this method, the current level of intelligence contained within the dynamic NN and knowledge from the on-line sensors are combined to make the best possible decision about the severity of wear on the tool. The dynamic network can also follow any progression of tool wear.

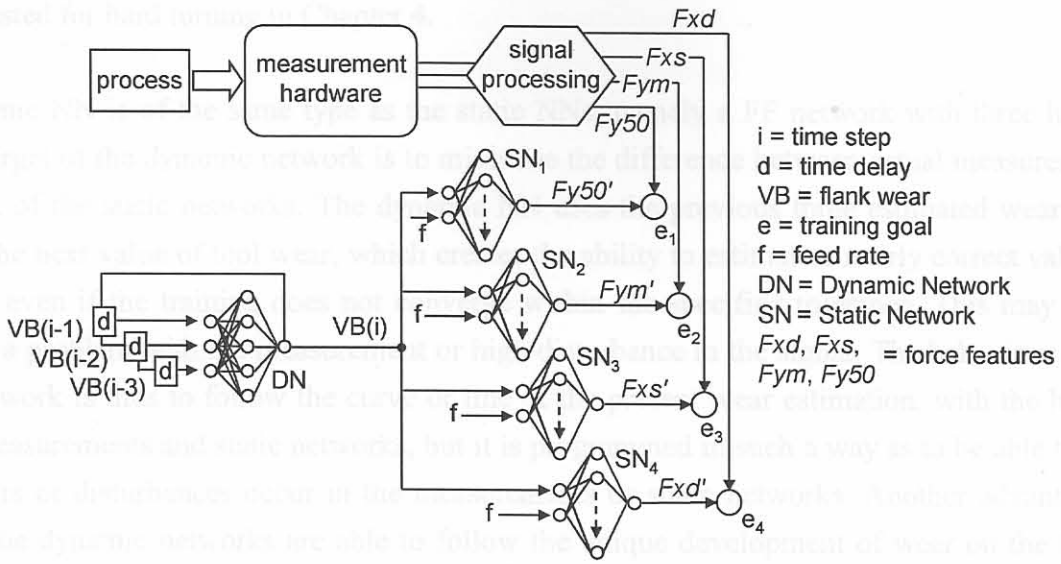

Figure 5.33: Monitoring strategy

5.7.1 Static networks

The static networks were trained, validated and tested for each of the chosen features. The data from eight cases of tool wear from a new to a worn tool insert was used as the training set. Two different cases of feed rate were considered and hence the feed rate was included in the static NN. The feed rate was excluded from the dynamic NN, with the assumption that the feed rate will only be changed with a new insert. Four relatively small static networks are used, all of which are FF networks with three layers. The middle layer consists of five 'tansig' neurons, and the output neuron has a linear activation function. The 'tansig' function is a combined tan and sine function. The static networks were trained with Levenberg-Marquardt backpropagation.

One of the most important considerations when training NNs is to prevent overtraining. This will cause the networks to memorise the training data and as a result they not be able to generalise when they are presented with new data. In this case, a combination of using small networks and early stopping were used to prevent this effect.

5.7.2 Dynamic network

With the static networks trained, the dynamic network is trained on-line to estimate the on-line value of the tool wear *VB(i)*. One of the main reasons why this approach is so efficient for TCM applications is the fact that tool wear almost never follows the same geometry and growth rate. If the static networks are trained appropriately, the dynamic network can follow any growth and geometry of tool wear. The dynamic network estimates the unknown parameter, namely tool wear, by using recent information obtained from the process. For this application, machining parameters did not change during the life of a tool and were consequently not included. However, any changing parameter that has a significant influence on the features can be included, for instance cutting speed, workpiece material or working angles. Another wear mode can also be included, for example flank wear and crater wear, as was suggested for hard turning in Chapter 4.

The dynamic NN is of the same type as the static NNs, namely a FF network with three layers. The training target of the dynamic network is to minimise the difference between actual measurements and the output of the static networks. The dynamic NN uses the previous three estimated wear values to estimate the next value of tool wear, which creates the ability to estimate a nearly correct value for the tool wear even if the training does not converge within the specified tolerance. This may happen if there was a problem with the measurement or high disturbance in the signal. The behaviour of the dynamic network is thus to follow the curve or line of the present wear estimation, with the help of the on-line measurements and static networks, but it is programmed in such a way as to be able to generalise if errors or disturbances occur in the measurements or static networks. Another advantage is the fact that the dynamic networks are able to follow the unique development of wear on the tool insert through on-line training (also refer to Section 4.6.3).

The method utilises sets of inner and outer steps or time-increments. The inner steps are training steps of the dynamic NN to achieve a specified convergence. Hence, during the inner steps, the tool wear is assumed constant and the NNs attempt to estimate this value. When this is achieved, an outer step is taken, and in this case it is an incremental step in the tool wear.

The problem can be described by considering a vector $\mathbf{x}$ containing the network bias and weight values of the Dynamic Network (DN):

$$\mathbf{x} = [x_1\ x_2 \ldots x_n] \tag{5.19}$$

In order to increment an outer step, the following optimisation problem must be solved, which is the training goal of the DN:

$$\text{minimise } f(\mathbf{x}) = \sum_{j=1}^{4} e_j \text{ such that } f(\mathbf{x}) \le tol \tag{5.20}$$

with the initialisation space for a new tool starting at:

$$D = \left\{ (x_1 \ldots x_n) \in \Re^n : -1 \le x_i \le 1,\ i = 1..n \right\} \tag{5.21}$$

and *tol* a suitable convergence tolerance on the function value. The initialisation space for a worn tool is obtained from the solution of the previous outer step. The error functions in equation 5.20 are de-

fined as:

$$e_1 = \sqrt{(Fy50' - Fy50)^2}$$
$$e_2 = \sqrt{(Fym' - Fym)^2}$$
$$e_3 = \sqrt{(Fxs' - Fxs)^2} \qquad (5.22)$$
$$e_4 = \sqrt{(Fxd' - Fxd)^2}$$

*Fy*50', *Fym*', *Fxs*' and *Fxd*' are the outputs of the static networks $SN_{1...4}$. When the DN reaches its training goal, an outer step can be taken and new values for *Fy50, Fym, Fxs* and *Fxd* can be measured using the on-line hardware and software. Note that all variables are normalised before they are entered into the NNs, and again de-normalised at the network output for interpretation of the results.

Similar to Chapter 4, it was found that the Particle Swarming Optimisation Algorithm (PSOA) yielded the best result for training the DN. Training NNs is in essence an unconstrained global optimisation problem, and recent literature also states that the PSOA outperforms methods like Genetic Algorithms (GAs) in unconstrained global optimisation. Furthermore the method is easy to implement and computationally efficient. The PSOA simulates the physical movement of social creatures, for instance the movement of a flock of birds. The algorithm does not utilise gradient evaluations and its efficient use of random information is advantageous for training NNs. A detailed formulation of the training algorithm is included in Appendix D. The algorithm usually achieved convergence within less than about 10 inner steps in a matter of seconds on a PIII computer. The convergence criterion was set on the function value. If convergence is not achieved within 10 steps, the training also terminates.

5.7.3 Discussion

It should be kept in mind that the aim of NN modelling should never be to make estimations outside the range of training. A NN should always be properly trained for its range of application. The most important part of the training is to ensure proper generalisation capabilities of the network. The network structure should be optimised to ensure that the network size and functions are chosen correctly for the application. In the case of the network size, iterations with different network sizes were used to choose the optimal network size. The result was quite small networks with adequate generalisation capabilities with respect to the problem. The network type and functions were selected by using proper judgement and experience with different types of NNs. The same arguments apply to the static and the dynamic networks. Further discussions can be found in Chapter 6.

5.8 Tool wear estimation results

5.8.1 From a new to worn tool insert

Results from the AI method with on-line estimations with previously unseen data for four tools is shown in Figure 5.34. In each case, the estimation starts with a new tool and ends when the operator removed the tool from the machine. The estimations are also compared with flank wear measurements taken under a microscope. It can be seen that there is a very good agreement between the estimation and the actual value of tool wear. Disturbances on the features also cause the estimated growth of tool

wear to appear somewhat noisy, but much less than that compared to the features. In two of the cases the flank wear exhibits the typical *initial fast* and *regular* wear stages. The tool is normally removed before the *accelerated final* wear stage and subsequent tool breakage is reached. However, it can be seen that the progression of tool wear, or the wear growth rate, is different for every case.

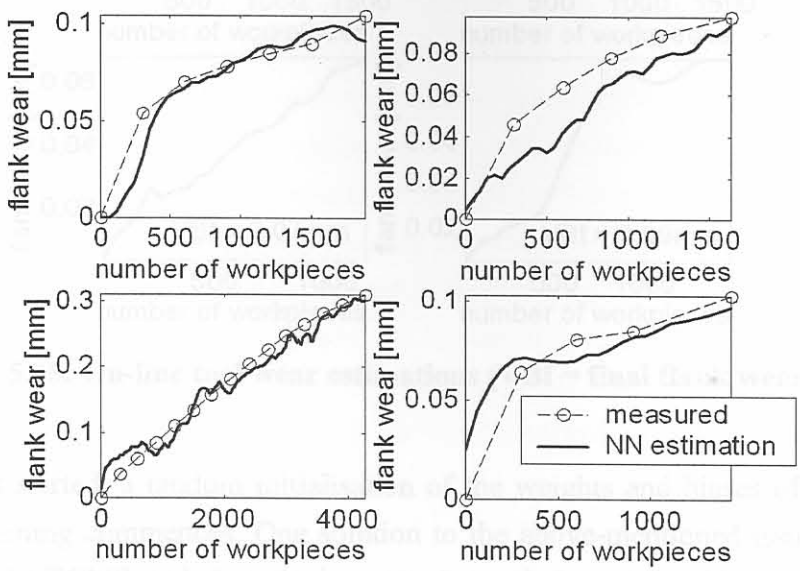

Figure 5.34: Tool wear estimations for four tools

The output of the dynamic NN is reported in terms of a "sliding output window" which means that an average value is taken that moves along with the outer steps. It was found that taking three averages is adequate. The usage of a sliding output window also helps to eliminate the possibility of making a decision based on only a single measurement that may contain errors. Many other examples of tool wear estimations are available, but these can only be compared to the final value of tool wear, because regular tool wear measurements could only be made for a limited number of tools. Four examples of online tool wear estimations are Figure 5.35. These can be compared to the final value of tool wear, and again a very good agreement is visible. The same observations regarding the growth rate of the flank wear can be made from these graphs.

5.8.2 Previously worn insert

In the previous section it was shown that the dynamic NN could estimate the tool wear accurately for a new insert that is allowed to wear normally. It should be kept in mind that the dynamic NN would tend to estimate the next value in the series of the previous three values of tool wear. The question then arise how the dynamic NN would react in the following two cases:

- If the tool is changed from a severely worn insert to a new insert
- If a worn insert is used from the start

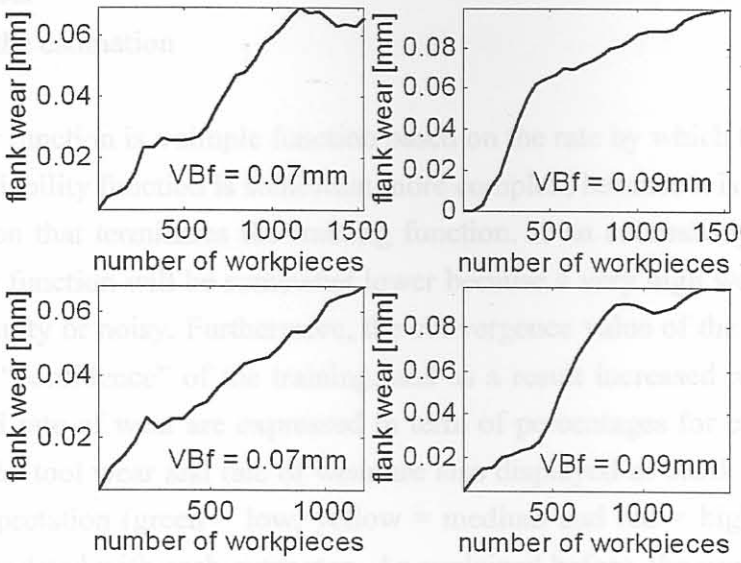

Figure 5.35: On-line tool wear estimations (VBf = final flank wear value)

When the TCMS is started, a random initialisation of the weights and biases of the dynamic NN is used after which training commences. One solution to the above-mentioned issues could be that the operator must reset the TCMS each time the insert is changed. A reset would cause the random initialisation of the dynamic network. Another solution is automatic detection of a new insert. Checking the output of the dynamic NN to see if it estimates a much lower value than before, towards 0 mm flank wear, could do this. The automatic detection proved to work very well. However, a manual reset is also included in the final implementation. An example of an estimation with the automatic detection and reset during a tool change with a new insert is shown in Figure 5.36a). When a worn insert is changed with a worn insert, the system must also react to quickly converge to the correct value of the tool wear. An example of a tool change with a worn insert is shown in Figure 5.36b). It is clear from the figure that the dynamic NN only requires a few steps to converge to the correct value of tool wear.

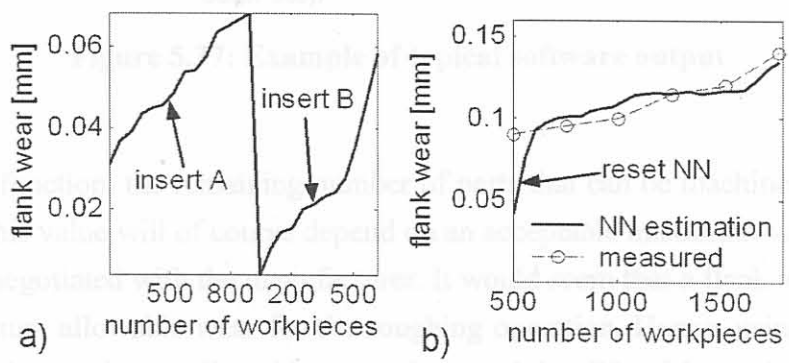

Figure 5.36: Dynamic NN response

5.8.3 Accuracy and reliability

A very important aspect of this development is the accuracy and reliability of the complete system. In terms of the reliability of the software, it was decided to also implement two additional functions that the end user can easily interpret when making a decision about the tool wear. These two functions are:

- rate of tool wear
- reliability of the estimation

The rate of tool wear function is a simple function based on the rate by which the estimated wear value is increasing. The reliability function is somewhat more complex, because it is based on the rate of tool wear and the criterion that terminates the training function. If an excessively high wear rate is estimated, the reliability function will be somewhat lower because a very high wear rate can be estimated if the input data is faulty or noisy. Furthermore, the convergence value of the training algorithm gives an indication of the "confidence" of the training, and as a result increased reliability. The reliability value, tool wear, and rate of wear are expressed in term of percentages for easy interpretation by the machine operator. The tool wear and rate of wear are also displayed as block diagrams and are colour coded for easy interpretation (green = low, yellow = medium and red = high). The percentages and block diagrams are updated with each outer step. As explained before, the user can select the tempo of outer steps with one outer step per workpiece the maximum. An example of the on-line software output is shown in Figure 5.37. Typically, when "flank wear" reaches 80% deviations in product quality can be expected.

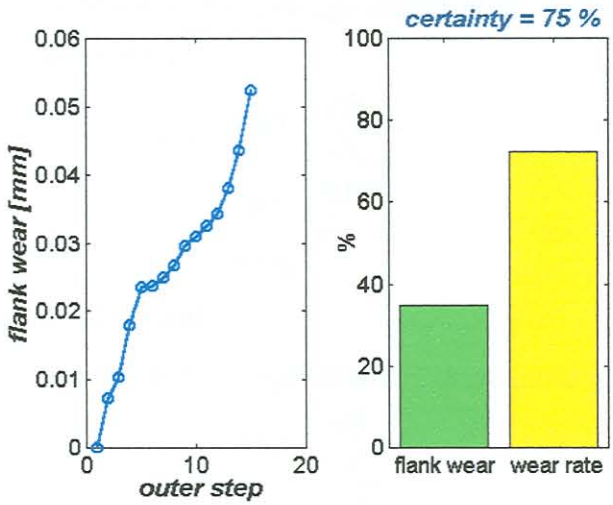

Figure 5.37: Example of typical software output

Using the wear rate function, the remaining number of parts that can be machined with the tool insert can be calculated. This value will of course depend on an acceptable maximum value of tool wear, and this will have to be negotiated with the manufacturer. It would seem that a flank wear of up to 0.25mm would be the maximum allowable wear for the roughing operation. Hence, using the estimated wear rate and 0.25mm as the maximum allowable wear, the remaining life of the tool can be calculated and updated with each outer step.

The accuracy of the tool wear estimations can be compared to the full range of observed flank wear, or to the current range of the particular tool. Furthermore, the average accuracy of the system can be compared to the minimum accuracy, thus the average deviation from the true tool wear and the maximum deviation. The following definitions can be made to describe the accuracy of the TCMS:

$$\text{Full range of flank wear } VB_{fr} = 0.31\text{mm} \tag{5.23}$$

$$\text{Maximum deviation from true wear } VB_{md} = 0.052\text{mm} \tag{5.24}$$

$$\text{rms deviation from true wear } VB_{rms} = 0.085\text{mm} \tag{5.25}$$

$$\text{1\% of full range } VB_{fr1\%} = {VB_{fr}}/{100} = 0.0031\text{mm} \tag{5.26}$$

These values were obtained from the results of all the data.

The rms deviation can be described as:

$$VB_{rms} = \frac{\sum_{i=1}^{n}\sqrt{\left(VB_{TCMS} - VB_{true}\right)_i^2}}{n} \tag{5.27}$$

where

n = the total number of tool wear measurements

VB_{true} = the measured tool wear

VB_{TCMS} = the wear estimated by the monitoring system

The following calculations are based on the average results of all the experiments. The average accuracy with respect to full range of wear is:

$$\begin{aligned}\eta_{Afr} &= 100 - \frac{VB_{rms}}{VB_{fr1\%}} \\ &= 100 - \frac{0.0085}{0.0031} \\ &= 97\%\end{aligned} \tag{5.28}$$

where $VB_{fr1\%}$ is one hundredth of the full range.

The minimum accuracy with respect to full range of wear can be calculated as:

$$\begin{aligned}\eta_{Mfr} &= 100 - \frac{VB_{md}}{VB_{fr1\%}} \\ &= 100 - \frac{0.052}{0.0031} \\ &= 83\%\end{aligned} \tag{5.29}$$

The average accuracy with respect to current range of wear is somewhat more complex but can be calculated with:

$$\begin{aligned}\eta_{Acr} &= 100 - \frac{1}{n}\left(\sum_{i=1}^{n}\frac{\sqrt{\left(VB_{TCMS} - VB_{true}\right)_i^2}\times 100}{\left(VB_{true}\right)_i}\right) \\ &= 92\%\end{aligned} \tag{5.30}$$

The minimum accuracy with respect to current range of wear can be written as:

$$\begin{aligned}\eta_{Acr} &= 100 - \frac{VB_{md}\times 100}{VB_{true}} \\ &= 100 - \frac{0.052\times 100}{0.16} \\ &= 100 - 32.5 \\ &= 68\%\end{aligned} \tag{5.31}$$

From the accuracy calculations the conclusion can be made that the system will estimate the true tool wear with an accuracy of above 92% as an average, and in extreme cases with accuracy not lower than 68%. The extreme cases rarely happen and in these cases the reliability index on the computer implementation will advise the user that the estimation could be inaccurate. It is important to mention here that the approach of measuring and monitoring was tested under shop floor conditions with different clamping conditions of the tool and workpieces over several months. Furthermore, the machines was completely stripped and serviced during tests. Different sensor-integrated tools were tested and none of these changes had a significant influence on the system. It can thus be concluded that the method is insensitive towards such changes and can be expected to always operate within the calculated range of accuracy.

5.9 Conclusion

This chapter described the implementation of a TCMS on the shop floor using AI. It was shown that the technique proposed is very effective for estimating the flank wear of tool inserts using features derived from strain gauge measurements. Features representative of tool wear are generated from both static and dynamic parts of the force signals. A combined static and dynamic NN technique was used with the PSOA method to train the DN. The method proved to be a very effective algorithm for training the DN. The system was developed and tested in a production environment, proving that such systems could run effectively on shop floor situations, despite the many disturbances present on the shop floor. An advantage of the system is its cost-effectiveness, due to the use of simple sensors and electronics. Another advantage of this approach is the fact that the tool wear is not accelerated, but it is allowed to run through its normal life, and hence it describes a normal wear pattern. It was also shown that the system is exceptionally accurate in estimating the true wear on the cutting tool. This approach proposed here can be modified to include any other parameters that might influence the features or growth of tool wear, and can also be applied to other machining operations if appropriate features can be generated. The method is not sensitive towards the clamping condition of the tool or other vibrational effects of the machine tool.